Journal Pre-proof

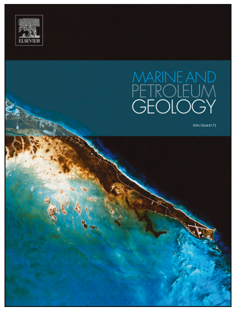

Characterisation of submarine depression trails driven by upslope migrating cyclic steps: Insights from the Ceará Basin (Brazil)

Daniele Maestrelli, Vittorio Maselli, Benjamin Kneller, Domenico Chiarella, Nicola Scarselli, Paola Vannucchi, Luigi Jovane, David Iacopini

PII: S0264-8172(20)30074-X

DOI: https://doi.org/10.1016/j.marpetgeo.2020.104291

Reference: JMPG 104291

To appear in: *Marine and Petroleum Geology*

Received Date: 25 February 2019

Revised Date: 28 January 2020

Accepted Date: 7 February 2020

Please cite this article as: Maestrelli, D., Maselli, V., Kneller, B., Chiarella, D., Scarselli, N., Vannucchi, P., Jovane, L., Iacopini, D., Characterisation of submarine depression trails driven by upslope migrating cyclic steps: Insights from the Ceará Basin (Brazil), *Marine and Petroleum Geology* (2020), doi: https://doi.org/10.1016/j.marpetgeo.2020.104291.

Characterisation of submarine depression trails driven by upslope migrating cyclic steps: insights from the Ceará Basin (Brazil)

Maestrelli Daniele[1], Maselli Vittorio[2], Kneller Benjamin[3], Chiarella Domenico[4], Scarselli Nicola[4], Vannucchi Paola[4,5], Jovane Luigi[6], Iacopini David[3,7].

[1]Consiglio Nazionale delle Ricerche, Istituto di Geoscienze e Georisorse (CNR-IGG), Via G. La Pira 4, Firenze, Italy

[2]Department of Earth and Environmental Sciences, Life Sciences Centre, Dalhousie University, 1355 Oxford Street, Halifax, Nova Scotia, B3H 4R2, Canada

[3]Department of Geology and Petroleum Geology, University of Aberdeen, King's college, Aberdeen AB24 3DS, UK

[4]Department of Earth Sciences, Royal Holloway, University of London, Egham Hill, TW20 0EX, UK

[5]Dipartimento di Scienze della Terra, Università di Firenze, Via G. La Pira, 4, 50121, Italy

[6]Instituto Oceanográfico, Universidade de São Paulo, Praça do Oceanográfico, 191, 05508-120, São Paulo, Brazil

[7]Dipartimento di Scienze della Terra, dell'Ambiente e delle Risorse, Università degli Studi di Napoli Federico II, via vicinale cupa Cintia 21, Naples, Italy.

Abstract

Circular to elliptical topographic depressions, isolated or organized in trails, have been observed on the modern seabed in different contexts and water depths. Such features have been alternatively interpreted as pockmarks generated by fluid flow, as sediment waves generated by turbidity currents, or as a combination of both processes. In the latter case, the dip of the slope has been hypothesized to control the formation of trails of downslope migrating pockmarks. In this study, we use high-quality 3D seismic data from the offshore Ceará Basin (Equatorial Brazil) to examine vertically stacked and upslope-migrating trails of depressions visible at the seabed and in the subsurface. Seismic reflection terminations and stratal architecture indicate that these features are formed by cyclic steps generated by turbidity currents, while internal amplitude anomalies point to the presence of fluid migration. Amplitude Versus Offset analysis (AVO) performed on partial stacks shows that the investigated anomalies do not represent hydrocarbon indicators. Previous studies have suggested that the accumulation of permeable and porous sediments in the troughs of vertically stacked cyclic steps may create vertical pathways for fluid migration, and we propose that this may have facilitated the upward migration of saline pore water due to fluid buoyancy. The results of this study highlight the importance of gravity-driven processes in shaping the morphology of the Ceará Basin slope and show how non-hydrocarbon fluids may interact with vertically stacked cyclic steps.

Keywords: sediment waves; cyclic steps; vertical fluid migration; turbidity currents; seismic geomorphology; Ceará Basin; Brazil

1. Introduction

The study of fluid migration in marine sediments has attracted considerable attention among geoscientists due to its importance in predicting the presence of deep-seated hydrocarbon reservoirs and in understanding the seal capacity and physical properties of specific stratigraphic intervals (Hovland 2003; Judd and Hovland, 2009). Circular to elliptical topographic depressions, with diameters ranging from hundreds of metres to a few kilometres and depths up of hundreds of metres, have been observed on the modern seabed at different water depths and ascribed to the vertical migration of fluids or gas (i.e. pockmarks; King and MacLean, 1970; Hovland et al., 2002;

Loncke et al., 2004). Fluid migration may take place due to pure overpressure mechanisms, overburden decompression due to sea level fall, seabed erosion, or destabilization of gas hydrates (Plaza-Faverola et al., 2011; Krämer et al., 2017; Bertoni et al., 2019). Fluids can be sourced from deep-seated hydrocarbon reservoirs (Heggland, 1998; Løseth et al., 2011; Maestrelli et al., 2017) or from shallow stratigraphic intervals due to diagenesis, formation of biogenic gas, or dewatering of channel-fill sands and mass-transport deposits (Davies, 2003; Meadows and Davies, 2007; Pilcher and Argent, 2007; Gay et al., 2007; Taviani et al., 2013). Alternatively, where there is no primary evidence of fluid migration, such as gas-charged sediments or fluid pipes, turbidity currents have been considered as a leading process in the formation of seabed depressions. Seminal works in the Monterey canyon, offshore California, illustrated how turbidity currents showing streamwise alternations between sub- and super-critical flow regimes may generate circular to elliptical seabed features, namely cyclic steps (Fildani and Normark, 2004; Fildani et al., 2006). Several studies have subsequently highlighted that cyclic steps can migrate both down-slope and up-slope and that can be generated through erosion, deposition, or a combination of both processes (Cartigny et al., 2011; Fildani et al., 2013; Cartigny et al., 2014; Covault et al., 2014; Garcia et al., 2016; Symons et al., 2016; Carvajal et al., 2017). On the Brazilian margin, Heiniö and Davies (2009) described how turbidity currents interacting with discontinuities in the topography of deep-water channels triggered the formation of sediment waves that evolved into circular depressions up to ca. 100 metres deep. Similarly, Lonergan et al. (2013) proposed that gullies and sediment waves associated with surface depressions on the upper slope region offshore Gabon were formed by mud-rich sheet-like turbidity currents showing lateral changes in the flow velocity. On the continental margin of Equatorial Guinea, vertically stacked circular depressions have been observed in the late stage infill of submarine canyons and interpreted to record a series of cyclic steps generated by diluted turbidity currents that evolved into pockmark trails during the passive infill of abandoned canyons (Jobe et al., 2011). In a recent study, Ho et al. (2012b, 2018) showed how the stacking of sediment waves generated by turbidity currents may interact with fluid migration, providing pathways for the upward migration of hydrocarbon-rich fluids that promote the formation of downslope migrating seabed depressions referred to as advancing pockmarks. In the present study, we use high-quality 3D migrated and stacked seismic data from the offshore Ceará Basin (Equatorial Brazil) to describe sedimentary depression features, often organized in trails, observed at the seabed and in the stratigraphy underneath. We characterise the internal architecture and the distribution of amplitude anomalies of the near-surfaced (< 1.5 s) stratigraphic intervals to provide a possible evolutionary model of the margin, discussing differences and similarities with sedimentary features previously reported in other settings.

Our results highlight the importance of gravity-driven processes acting on the Ceará Basin slope, showing how they are capable of shaping its morphology and drive its evolution during Neogene, interacting with migration of non-hydrocarbon fluids and creating permeable pathways through the staking of cyclic steps depression.

2. Regional geology and study area

The study area is located in the Mundaú sub-Basin (Fig. 1) which is part the offshore sector of the Ceará Basin (Brazilian Equatorial margin, BEM; Jovane et al., 2016). The Brazilian Equatorial margin started to develop in the Early Cretaceous due to breakup of the Gondwana super-continent (Asmus and Porto, 1972; Morihak et al., 2000). The South Atlantic rift system is bounded to the north by the transcurrent fault system associated with the Romanche Fracture Zone (RFZ) and to the south by the Malvinas Plateau (MP; Fig.1). The RFZ is a linear fracture zone with an average width of approximately 16 km that extends over 4,500 km from offshore northern equatorial Brazil to its conjugate African margin offshore Ghana and Togo/Benin (Davison et al., 2015). The Ceará Basin developed during three tectonic stages, rift (Berriasian-Aptian), post-rift (Aptian-Albian), and continental drift (Albian–Holocene), each recorded by mega-sequences composed of continental, transitional, and marine deposits, respectively (Matos, 2000). Well CES-112 is located in the north-western corner of the study area (see green dot in Fig. 1; Conde et al., 2007) and provides broad constraints on the Neogene stratigraphy of the Ceará margin (Jovane et al., 2016).

From an oceanographic point of view, water circulation on the narrow continental shelf is dominated by the North Brazil Current (NBC), which flows almost parallel to the coast from SW to NE (Vital et al., 2010). The NBC is a combination of shelf-parallel and tidal currents that together may reach velocities of up to 40 cm s^{-1} (Vital et al., 2010; de Almeida et al., 2015). At depths of around 4,600 metres, the BEM is affected by the Deep Western Boundary Current (DWBC), which brings the North Atlantic Deep Water (NADW) towards the south at speeds of up to 30 cm s^{-1}.

3. Data and Methods

3.1. 3D seismic datasets & interpretation

The study makes use of two high-quality 3D seismic surveys acquired in 2009 and provided by PGS and CGG. The PGS survey (white polygon in Fig. 1) is a full stack, Kirchhoff time-migrated reflection seismic volume covering an area of ~1,600 km^2. The volume has a line spacing of 12.5 m in both in-line and cross-line directions and a vertical sample interval of 2 milliseconds (ms). The data are zero-phase processed and displayed so that an increase in acoustic impedance is represented by a blue-red-blue reflection loop (SEG normal polarity; e.g., Veeken and Moerkerken, 2013). Amplitude values were normalized and rescaled to constrain maximum and minimum values between +1 and -1. The dominant frequency of the section of interest ranges between 30 and 60 Hz. A sound velocity of 1,500 m s^{-1} is used for seawater, and 1,800 to 2,500 m s^{-1} for the near-seabed interval of interest, calibrated using data from well CES-112 (Fig. 1). These velocities and frequencies correspond to a best vertical resolution (limit of separability $\lambda/4$, being λ the P-wave wavelength) of 6.5 m for the seabed and 7.5-15 m for the near-seabed units. Taking into account the focusing effect of Kirchhoff migration (Brown, 2004), a Fresnel zone radius of 11.6 m to 18 m is estimated, assuming the radius is equal to the average P-wave velocity/4F (with F=Frequency).

The CGG survey lies within the above volume over a smaller area of 500 km^2 and consists of three Kirchhoff time-migrated seismic partial stacks (near-, mid-, and far-field trace) volumes. The three partial stack volumes were used to perform qualitative amplitude analysis along two seismic sections corresponding to profiles L5a and L5b (see location in Fig.1). The partial stack data were processed using an amplitude preservation procedure that included geometric spreading corrections and preserved amplitude pre-stack time migration (PSTM). The character of the wavelet was used to correct the near-stack to zero phase. The frequency content ranges between 30 and 50 Hz, depending on the near to final stacks. The partial stack seismic data were used to extract and map the amplitude response across specific depression trails.

In a subset of the data (orange dashed rectangle in Fig. 1), time structure maps of key horizons were generated using standard seismic interpretation techniques (Figs. 2, 3). These maps are displayed as grids of two-way travel time values with a sample size of 12.5 × 12.5 m (Fig. 4).

3.2. AVO analysis on partial stacks

Amplitude Versus Offset (AVO) analysis was applied to investigate the bright and weak anomalies associated with the depression trails investigated in this study (Castagna et al., 1998). The three partial stack volumes (near-, mid-, and far-field trace) were re-processed following a robust workflow for amplitude preservation and noise suppression (Ross and Beale, 1994). An analysis of seismic data quality and data conditioning similar to that proposed by Efthymiou et al. (2010) was performed to explore systematic background phase and frequency changes across the partial stacks. The phase was corrected by applying filters designed to match the seismic far-stack to the near-stack. Instantaneous frequency attributes were used to analyse and compare frequency changes across the two partial stack volumes (Taner et al., 1994). Time alignment was performed to explore and correct any misalignments. Only those portions of the partial stack data with a minimum time shift and misalignment were considered for analysis. The AVO reflectivity was described using a modified version of the Aki and Richards (1980) equation simplified for small angles. The equation was interpreted in terms of different angular ranges using the Castagna (1993) expression, where gradient and intercept from partial stacks are calculated using range stack profiles and adopting the following expressions:

$$\text{Gradient} = \frac{(R(\theta_f) - R(\theta_n))}{(Sin\theta_f^2 - Sin\theta_n^2\ )} \quad (1)$$

$$\text{Intercept} = R(0) = R(\theta_n\ ) - Gradient * (sin\theta_n^2) \quad (2)$$

The angles θ_n and θ_f represent the near- and far- angle stacks (average angles are 5 and 15 degrees) and the values are plotted across a gradient versus intercept volume.

In order to obtain reflectivity values, envelope attributes across the area of interest were calculated and envelope volumes attributes for each of the partial stacks that represent the values R(θ_n) were generated. The near-, mid-, and far-field stacks volumes represent the main input to calculate gradients using equations (1) and the intercept using equation (2). The angle values for each partial stacks are assigned as central values (obtained from the pre-stack report) to each of the partial stack volumes. The calculated gradient and intercept values are plotted using a simple scatter plot gradient versus intercept, as proposed by Castagna and Swan (1997). For all anomalies, the selected bright amplitudes were sampled along with the adjacent lower amplitudes (along the same reflector) required to create the background distribution necessary to analyse the AVO data.

Amplitudes were analysed in small windows (minimum size of 10×10×10 3D cells, i.e., “voxels”) to reduce the background noise that is known to cause problems during the detection of possible gas trends.

4. Results

4.1. Seismic stratigraphy and key seismic horizons

The 3D seismic bathymetry shows that the seabed (SB) in the study area (Fig. 1, covering an area of ~465 km^2) lies at about 100 metres water depth at the shelf edge, dropping to more than 2000 metres toward the continental rise, with an increase of gradient from 1° to more than 3° downslope (Fig. 1). The seabed is characterised by two deep canyons (up to 2 km wide) that incise the shelf edge and a number of straight small channels (~500-600 m wide) that form in the upper slope and are often associated with sediment waves (Fig. 1). In addition, the seabed includes a variety of circular to elliptical topographic depressions either as isolated features or organized in trails (i.e. aligned depressions, often observed inside channels; Fig. 1).

The stratigraphy of the study area was investigated using the 3D seismic data, after correlation with Well CES-112. The well was correlated with key seismic horizons identified in this study, allowing us to subdivide the Neogene into two main units (Fig. 2), here named the "Upper Bedform Unit" (UBU) and the "Lower Channelized System Unit" (LCSU). The sediments at the base of LCSU are estimated to be post upper-Miocene in age. The two seismic units were identified based on seismic reflection architecture, mapping four seismic horizons (from top to bottom, the seabed SB, H3, H2 and H1; Fig. 4a,b,c,d) that delimit -or are included in- the above mentioned units. Horizons H1 to H3 were mapped due to their significance for the analysis of depressions observed at the seabed (SB, Fig. 2).

The UBU lies between the seabed SB and horizon H1, and includes horizons H2 and H3. UBU is characterised by undulating sediment waves, ca. 150-200 m in length, and by isolated depressions and depression trails (Figs. 1, 4). The unit is cut by two canyons, their thalwegs marked by a yellow line on the horizon maps of Figure 4.

The LCSU lies beneath horizon H1 and is characterised by amalgamated channel systems locally intercalated with mass transport deposits (Fig. 2c). As shown by the time structure map of H1, this unit contains trails of depressions and channels that extend across the area of interest.

Horizons H1 to H3 are distributed through the stratigraphic sequence in a depth range 300-600 ms below seabed (Figs. 2, 4). The seabed and horizons H1-H3 gently dip toward N-NE, where the maximum depth is between 3200-3500 ms (Fig. 4). In some places the horizons are discontinuous due to erosion by the large canyons (Fig. 4). The seabed horizon SB shows sediment waves (Fig. 4d), the geometry and internal architecture of which indicate upslope migration (Fig. 2). The wavelength and height of these bedforms are 250-500 metres and 10-50 metres, respectively (Fig. 2a, c). Between the two canyons, isolated circular depressions (red arrow in Fig. 4d; line L3 in Fig. 3a) and trails of elliptical depressions (orange arrow in Fig. 4d) are oriented downslope and aligned along small channels. The steep flanks of the canyons are eroded by small gullies or slope failures. Some of the isolated depressions in the area east of the main branch of the eastern canyon (white arrows in Fig. 4d) maintain the same position between the seabed and horizon H3. Horizon H3 (Fig. 2c) shows depressions both isolated and organized as trails along a channel-like feature (Fig. 4c). The isolated depressions tend to form broadly spaced trails or to merge into larger features with an elliptical geometry. Trails of depressions nucleate along pre-existing erosional channels (Fig. 4c) between the two large canyons (Fig. 5). The canyons and channels visible on horizon H3 maintain the same position as observed at seabed. Horizon H2 is characterized by sinuous bedforms (*sensu* Symons et al., 2016) with a wavelength of about 500 m, their crest marked by blue dashed lines in Figure 4b. Downslope of these bedforms, circular depression features are present in the intra-canyon area (Fig. 4b). This time structure map shows that the depression trails are widespread and interact with the sinuous bedforms. Horizon H1 is a prominent surface separating UBU from the underlying LCSU unit. On the H1 time structure map (Fig. 4a), it is possible to observe trails of depressions and channels that extend across the slope.

4.2. Lateral and vertical distribution of depressions relative to channels/canyons

Mapping of the four seismic horizons reveals the following key information: (a) the canyon features observed on H1 (Fig. 4a) represent the precursors of the main canyons observed at the seabed (Fig. 4d); (b) the canyons remained erosional features through time, while the inter-canyon areas continuously aggraded (Fig. 4); (c) both isolated depressions and linear trails of depressions are observed across the entire slope, along both the channels and the inter-channel areas (H1-H3 in Fig. 4 and Fig. 5). The observed seabed canyons have deep erosive walls, up to 200-300 metres in height, with little or no evidence of overspill deposits. Although at seabed and in the subsurface some of the depression trails appear isolated (SB in Fig. 4d), many others are localized along the axes of the smaller channels, both buried and active (Fig. 4, H1 to SB).

4.3. Characteristics of depression features

With a maximum diameter of 1 km, maximum depth of 300 m, and asymmetric internal flanks, the depressions occur either as circular to elliptical isolated features (arrow A in Fig. 1; Fig. 5), or in trails aligned downslope, in places developing a channel-like morphology (arrows B and C in Fig. 1; Fig. 2a; green arrow in Fig. 4c). Seismic profiles orthogonal or oblique to the slope (L1 in Fig. 2b; location in Fig. 4), show the depressions as a series of vertically stacked concave-up reflections of variable amplitude. As indicated in Figure 3 along different cross-sections (L1 to L4), these features show evidence of both aggradation on their walls and minor erosion on their walls and floors, as well as onlapping by sediment waves (arrows 9 and 14 along the line L4 in Fig. 3). Stacked depressions are characterized by local erosional surfaces marked by truncated reflections (Fig. 2b) typically bounded by continuous horizons (i.e. H2, H3, Fig. 3c). Some persist in almost the same position as observed on horizon H1, to appear as depressions on the seabed (Fig. 3a, b). In other cases, depressions are filled with sub-horizontal reflections that onlap the concave-upwards bounding surfaces with no seabed expression (Fig. 3c). At a closer scale of observation (Figs. 2b and 3c), stacking of concave-up reflections shows that successive aggrading packages, are displaced either (sub-) vertically or upslope (Fig. 3a, c). When not eroded, each package is commonly separated by a draping unit (Figs. 2b and 3c).

In summary, the topographic depressions are observed along the slope in association with upslope migrating sediment waves (Fig. 2a, c), and where aligned in trails (Fig. 5) a clear link can be observed with the slope channels (e.g., as observed on horizons H1 and H3 in Fig. 4).

4.4. Amplitude anomalies

Amplitude anomalies of positive and negative polarity are observed at different subsurface depths across the slope and within different sedimentary features. No bottom simulating reflectors (BSRs) are observed. Seismic profiles from the full stack dataset reveal a clear correspondence between stacked positive amplitude anomalies (arrows 1 and 3 in Fig. 2b; arrow 6 in Fig. 3a, b), negative amplitudes anomalies (arrows 4, 5, 7, 8 in Fig. 3a, b; arrows 9 to 14 in Fig. 3c), and the depression features. Amplitude anomalies are observed within the passive infill of the depressions (arrow 3 in Fig. 2b; arrows 9 and 14 in Fig. 3c). Stacked anomalies with high positive amplitude but weaker than the seabed reflection are observed throughout the infill of the depression (arrow 1 in Fig. 2b). Besides, in places, seismic horizons with relatively high positive anomalies are observed within the draping infill of the depression (arrow 3 in Fig. 2b). Stacked depressions persisting up to the seabed are characterized by weak to strong (but less than the seabed), negative amplitude anomalies (arrows 4, 5, 7, 8 in Fig. 3a). Weak negative anomalies are observed to extend across depressions (arrows 7 and 11 in Fig. 3a, c), and in some cases are relatively flat (arrows 9, 14 in Fig. 3c). Strong negative anomalies are also observed in places between depression trails (arrows 12, 13 in Fig. 3c).

4.5. AVO analysis of amplitude anomalies

AVO analysis of 3D seismic partial stack data was undertaken at two sites, corresponding to positive and negative amplitude anomalies (Fig. 6). The selected anomalies are shown along two extracted seismic profiles (line L5a and L5b; trace location in Fig. 1), together with maps of their 3D spatial distribution (Figs 6b, d).

Weak positive anomalies (Fig. 6a) are stacked over a vertical range of 50 ms and their geometry has been mapped in detail (Fig. 6b), showing that at the investigated site, they have a concave-up, roughly circular, geometry, with a diameter of 150-200m. Maximum brightness is observed at the centre of the anomaly. Along the same reflector, far from the weak positive anomalies, amplitudes were sampled to define a background response of the same unit.

Negative anomalies (Fig. 6c) are observed at the base of a depression characterized by a clear upward migrating sediment wave. They have been mapped (Fig. 6d) and sampled similarly to the positive amplitudes, to analyse the AVO response. The 3D mapping showed geometry and dimensions similar to the above described positive anomaly, with the maximum brightness located at its centre. Analysis of the relative envelope values across both sets of anomalies and along the background units, using Equations (1) and (2), allowed calculation of the AVO gradient versus reflectivity cross-plots presented in Figures 6e, f. The plots are represented using the Castagna and Swan (1997) diagram (Fig. 6g).

The AVO cross-plot for the first anomalies in Figure 6e shows a single cloud trend from the sampling of the surrounding units (blue triangles), with a much larger spread for the bright amplitudes (green triangles) toward the Class I and Class IV (Fig. 6g) and a minimal shift of the point distribution towards the negative intercept. The AVO cross-plot in Figure 6f shows a similar pattern of the AVO plot of the depression trails observed in Figure 6a with the background values (green triangles) showing a single cloudy trend and a similar spread in their distribution. The anomalies themselves (red triangles) also show no shift toward lower gradient, but a large spread distribution along the diagonal of the gradient intercept. In both cases, we do not observe any distinct trend towards the negative reflectivity and negative gradient quadrant.

5. Discussion

5.1. Amplitude anomalies: depression infill vs fluid effects

In seismic reflection data, isolated amplitude anomalies (regardless of polarity) have several potential causes: changes in the sediment grain-size, cementation, or mineralogical composition as well as the the presence of fluids with properties significantly different from normal marine pore water (e.g. hydrocarbons or brines; Avseth et al., 2010). In addition, constructive and destructive interference near tuning thickness may mimic petrophysical responses (Barrett et al, 2017). In near-seabed stratigraphic units, where sand is unconsolidated and shale can be of higher acoustic impedance, strong negative anomalies of higher amplitude than the seabed reflection (bright spots) coupled to negative gradient and intercept values (Class II and III, see Castagna and Swan, 1997 and Fig. 6g) indicate the presence of gas within poorly consolidated sediments (Avseth et al., 2010). In areas where bright spots are present, fluid pathways like fluid-escape pipes, gas chimneys or fault intersections may also be visible. In the absence of fluid pathways, weak negative or positive anomalies cannot be unequivocally associated with the presence of fluids, but may be indicative of sediment cementation, composition, or grain-size changes (Jobe et al. 2011, Mavko et al., 2012).

Our analysis of amplitude anomalies within the concave-up floors of the depressions shows positive and negative anomalies with lower brightness than the seabed. None of the stacked depressions is affected by seismically visible fault or pipes. AVO analysis performed on two examples shows a clear and consistent distribution of background amplitudes, (blue triangles in Fig. 6e, green triangles in Fig. 6f) sampled laterally along the same reflector to characterise the reference sand/shale units.

The AVO diagram shows that the sampled positive and negative anomalies (green triangles in Fig. 6e and red triangles in Fig. 6f) are consistently distributed along the trend of the background sediments. With respect to the background sediments, the plot of the sampled anomalies shows small or no shift toward negative gradients, but instead a slight spread toward the Class I and class IV of the Castagna and Swan (1997) cross-plot (Fig. 6g). This distribution suggests that sandy and muddy sediments are mostly poorly consolidated and not affected by anomalous fluid saturation, ruling out gas and hydrocarbon fluids as the cause of the anomalies (Castagna and Swan, 1997; Foster et al., 2010).

These results require the exploration of alternative explanations for the presence of the anomalies. Possible hypotheses for relatively weak positive and negative amplitude anomalies stacked within the depressions include: a) vertical variation of grain-sizes (fine to coarse) and or some degree of compaction within the depressions (resulting in weak positive anomalies, Fig. 2b); b) presence of non-hydrocarbon fluids (saline pore waters, de-watering of unconsolidated pelite and shale sediments) characterised by weak gradient variation (Fig. 6e, f). If the sediments within the vertically stacked depressions are composed of unconsolidated sands of higher porosity and permeability, saline pore water could explain the negative amplitudes, the poor AVO shift, and the reduced spread of the cross-plotted AVO parameters (Fig. 6e; Foster et al., 2010 and Mavko et al., 2012). The latter could also be explained by a higher porosity and permeability reduced by fluid-depositing cement (Foster et al., 2010).

In view of these considerations, the positive amplitude anomalies observed in the depressions described in Figures 2b, 3c and 6a,b (e.g. arrows 1 to 3 in Fig. 2b) could be an expression of either grain-size variations or cementation effects. Ho et al. (2012b, 2018) suggested that the accumulation of coarse-grained and porous sediment during the vertical aggradation of consecutive depressions could create fluid migration pathways. We propose that this process may explain the observed weak to strong positive amplitude anomalies as an effect of variation in porosity or granulometry.

The same process proposed by Ho et al. (2012b, 2018) could account for the few locations where anomalies are negative and stronger, in terms of the preferential migration of saline pore waters.

5.2. Down-slope cyclic steps that nucleate in 'channels'

Observations of seabed morphology and subsurface stratigraphy show that sediment waves occur as groups of upslope-migrating and aggradational structures (as in Fig. 2c), which evolve along slope into circular and elliptical depressions (Figs. 1, 2a, 5), and that a clear link exists between the trails of elliptical depressions and both the sediment waves and emerging channels observed along H1 to H3 (Fig. 4).

These observations suggest that the sediment waves characterizing the depression trails can be ascribed to the formation of cyclic steps (*sensu* Cartigny et al., 2011) triggered by the passage of turbidity currents along the pathways created by coalescent depressions, similar to the model proposed by Heiniö and Davies (2009). The more isolated depressions experienced less (if any) erosion, being away from the main sediment routes. Flat high-amplitude fills are found within the continuous downslope trails of depressions (arrow 3 in Fig. 2b; arrow 9 in Fig. 3c). Sediment deposition, therefore, occurred in areas previously affected by energetic, and perhaps coarse-grained and high-density, turbidity currents (e.g., Talling et al., 2012). In contrast, concave-upwards fills, which tend to show only minor thickening into the depressions, suggest lower density, finer-grained turbidity currents, moving downslope away from the main sediment routes.

We propose the following conceptual model for the evolution of these structures (Fig. 7):

a) Deposition on the upper slope initiated as a series of sediment waves (SW in Fig. 2a) related to the passage of unconfined gravity-driven flows (arrow D in Fig. 1, UGDf in Fig. 2a, dashed blue line on H2, Fig. 4a; T1, Fig. 7;). In deep-water settings, gravity-driven flows such as turbidity currents are mainly generated by the following mechanisms: (1) river-fed hyperpycnal flows (Mulder and Syvitski, 1995); (2) impact of storm waves on the outer shelf and upper slope (Mulder et al., 2001; Puig et al., 2004); (3) sediment overflow from slope canyons (Normark and Hess, 1980); (4) landslides, slumps or debris flows (Hsu et al., 2008). With time, the passage of multiple gravity-driven flows led to the development of preferential seabed erosional pathways (highlighted by the truncation of seismic reflectors) amplifying the depressions.

b) Gravity-driven flows may interact with small-scale (tens to hundreds of metres) morphological variations of the sea floor or may involve spanwise instabilities within the flow itself (Hall et al., 2008; Heiniö and Davies, 2009; Lonergan et al., 2013); these processes can generate the randomly distributed depressions observed on the slope (T1 Fig 7; Fig. 4d and Fig. 5), and lead to the coalescence of some depressions into downslope trails (Figs. 2a, 4 and 5).

c) Depression trails were amplified and perpetuated as cyclic steps (CS in Figs 2a and 2c), a sedimentary bedform that has been recognized in many submarine canyons and channel systems worldwide (Normark et al., 2002; Fildani et al., 2006; Heiniö and Davies, 2009; Symons et al., 2016).

Finally, as described by Heiniö and Davies (2009) and Lonergan et al. (2013), some depressions were partially filled or even buried, as shown by onlap reflection terminations with varying amplitude (Line L4 in Fig. 3). Partial fill can produce different geometries ranging from sub-horizontal, abrupt onlap (arrows 2 and 3 in Fig. 2b) to concave-upwards infill packages with only minor thickening at the base of the depressions (arrow 1 in Fig. 2b, arrows 4 and 5 in Fig. 3a; Fig. 7, T2 to T3).

5.3. Depression trails vs pockmarks: comparison with existing models

Heiniö and Davies (2009) proposed a model for the formation of depression trails in the Espirito Santo Basin that suggests the role of density current along submarine channels in creating sediment waves and plunge pools, generating circular to elliptical trails of depressions. This model is consistent with our observations (cf. Fig. 11 by Heiniö and Davies, 2009), suggesting that the depressions are not pockmarks. Nonetheless, our amplitude analysis indicates that in the area of investigation there may have been some exceptions or concurrent mechanisms. Seismic amplitude analysis within the sedimentary succession shows that the concave-up fills of both isolated depressions and depression trails are associated with weak to bright amplitude anomalies from bottom to top. In some cases (arrows 4 to 8 in Fig. 3a; arrows 10, 11, 14 in Fig.3c), the concave-upward fills show weak to strong negative anomalies. In general, these anomalies can be related to any physical property of the material affecting its density and/or seismic wave velocity. We showed above, that AVO analyses rule out the presence of hydrocarbon fluids, suggesting that, amplitude anomalies are due to saline pore waters, simple de-watering mechanisms or to coarser grained/cemented sediments.

In a different context, Ho et al. (2012a,b; 2018) suggested an interplay between bottom currents and hydrocarbon leakage at the seabed, that may initiate and afterwards drive the pockmark evolution. In their model, the presence of hydrocarbons implies an active role of fluid overpressure in the formation and shaping of these features, which is controlled by turbidity currents and slope dip (Ho et al., 2018).

Our results provide no evidence that overpressured fluids including hydrocarbon were involved in the formation of the depression trails. Nonetheless, the onlapping nature of some of the rare main bright infill and draping reflections (arrow 9 and the flat lying reflector above arrow 14 in Fig. 3c) onto the erosive surface (dotted line in Fig. 2c) suggest that non-hydrocarbon fluids may have interacted with the cyclic erosional and depositional evolution of the depression: fluids that migrated out of depressions during erosion were trapped during phases of sedimentation and infill. Therefore, the depression trails in some cases may have acted as preferential pathways for vertical fluid migration, without being its direct product as in the case of pockmarks (Hovland et al., 2010; Ho et al., 2018). The complexity of the depositional environment as well as the ambiguous nature of the anomalies observed in the depression trail suggest that density currents along submarine channels creating sediment waves and plunge pools represent the main driver, but we do not rule out that in some cases other mechanisms may have been active during the Neogene development of the depression trails.

6. Conclusions

Analysis of 3D seismic surveys in the Ceará Basin, offshore Brazil, allows the description and characterisation of the processes shaping the Ceará slope. Our results highlight the presence of large erosive canyons developed throughout Neogene time, as well as inter-canyon aggrading areas marked by the presence of smaller channels. These features indicate a strong influence of confined and unconfined gravity-driven processes occurring along the slope, these latter being responsible for the formation of depressions at seabed. The depressions are present within the upper hundreds of metres of subsurface sediment and occur isolated or in trails, as observed in other slope settings. Although isolated depressions may resemble pockmarks, their internal stratal architecture and relation to host sediments supports the interpretation of such features as generated by upslope migrating cyclic steps, produced by gravity-driven turbiditic flows. In our area, Amplitude versus offset (AVO) analysis of positive and negative amplitude anomalies within the depressions excludes the presence of hydrocarbons, thereby confirming that the seabed depressions are not the result of fluid escape driven by overpressure.

However, some weak negative amplitude anomalies suggest that saline pore waters or fluids derived by sediment de-watering may be (or may have been) present within some of these vertically stacked depressions, exploiting them as passive fluid migration pathways, thanks to fluid buoyancy.

Therefore all our observations suggest that different players, such as slope sedimentation, seabed morphology, depression trails originated by gravity driven processes and possibly interacting with fluids, concur to the shaping of the Ceará Basin slope, and likely to other slope settings worldwide.

Declaration of interest

We declare that one of the authors (Domenico Chiarella) is an Associate Editor of Marine and Petroleum Geology journal.

Acknowledgments

We sincerely thank Petroleum Geo-Services (PGS), and specifically David Hajovsky and Opdyke (PGS) for releasing the 3D data (BMCE-2) used for the main interpretation analysis. CGG and C. Baron (CGG) are also thanked for furnishing their 3D full and partial stack data (BMCE 1&2) and allowed us to show these results. We kindly acknowledge the Associate Editor Daniel Praeg for his careful revision of the text and for the many useful comments that highly improved the quality of the manuscript. We thank three anonymous reviewers for their detailed and constructive reviews. We are grateful to M. Huuse and D. Duarte for their constructive comments on a previous draft, and to Bill Richards for the final review of the manuscript. D.M. was funded through the Tuscany PhD Regional program [grant POR ICO FSE 2014/2020-Asse C] and the Erasmus+ exchange for his visit in Aberdeen. The seismic interpretation was performed at the *SeisLab*, Department of Geology and Petroleum Geology (University of Aberdeen).

Figures and Figure captions

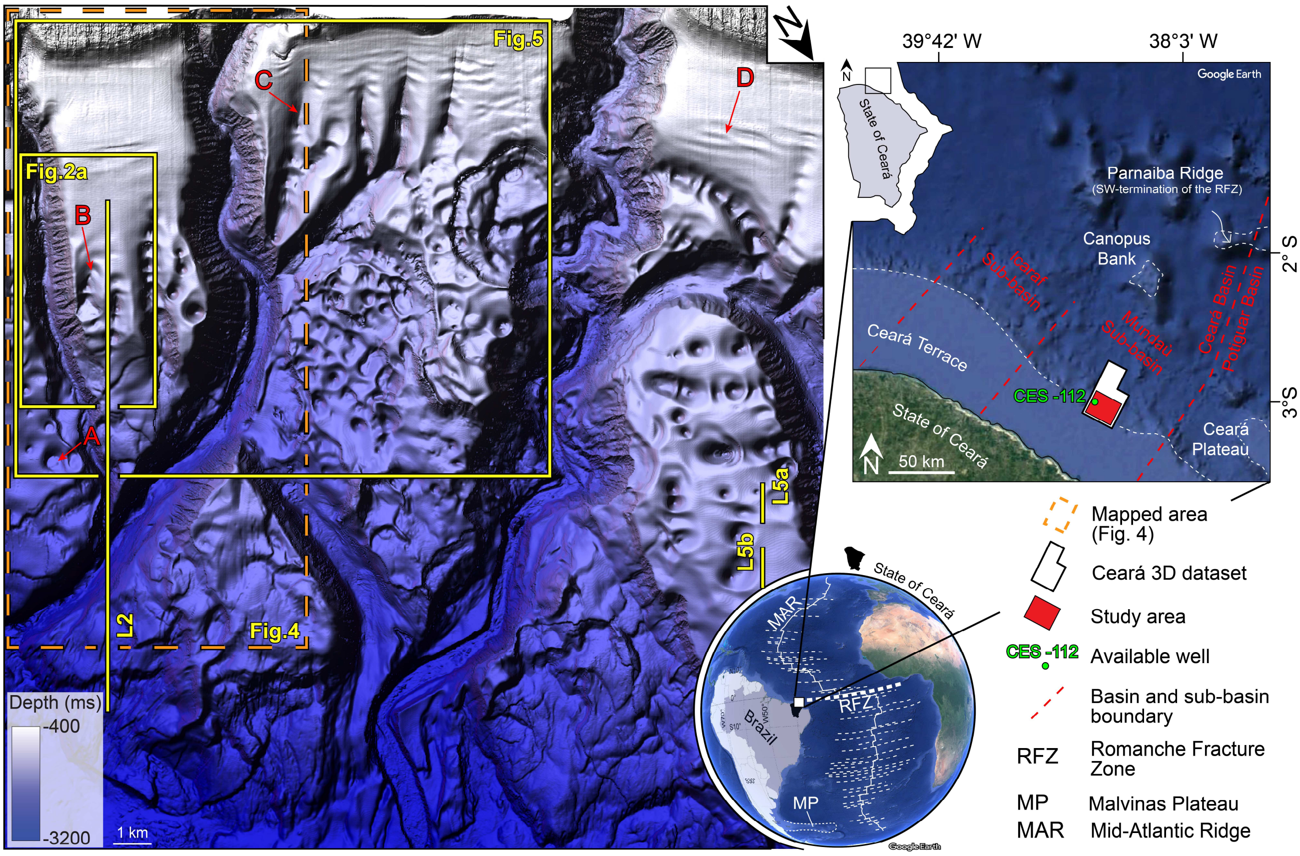

Figure 1. Right: location of the study area (red rectangle, covering an area of ~465 km^2) in the Mundaú sub-Basin, offshore Ceará Basin (Equatorial Brazil). The study area corresponds to part of the full 3D seismic dataset (white polygon) used in this study. Left: seabed bathymetry of the study area extracted from 3D seismic data. Arrow A: isolated pockmark-like structure; Arrow B: depression trails aligned parallel to the seabed gradient; Arrow C: elongated channel-like morphology; Arrow D: roughness of the paleo- seabed. Line L5a and L5b represent the traces of

seismic lines extracted from a second 3D dataset (partial stacks) used for Amplitude Versus Offset (AVO) analysis (see Fig. 6). Seismic line L2 is shown in Figure 2.

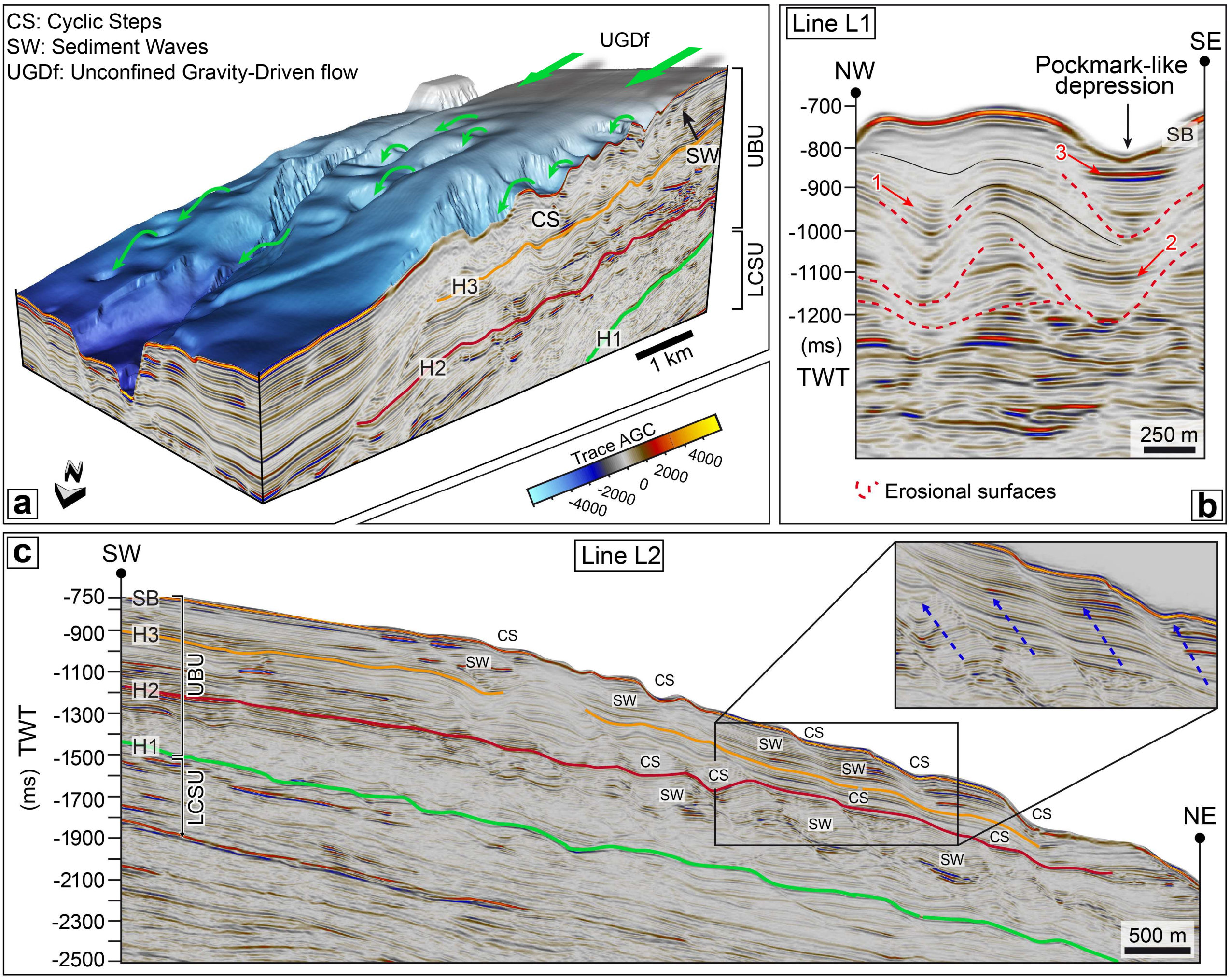

Figure 2. (a) 3D perspective view of seabed combined with seismic profiles (location in Fig. 1). The alongslope seismic section intersects a slope canyon, while the downslope section intersects a trail of depressions and shows a stepped seabed generated by upslope migrating Sediment Waves (SW) and Cyclic Steps (CS). UGDf: Unconfined Gravity-Driven flow, marked by large green arrows in (a). (b) Seismic line L1 (oriented alongslope, location in Fig. 4c) shows two stacked depressions culminating in a pockmark-like depression at the seabed. Note the amplitude anomalies (arrows 1 to 3). (c) Seismic line L2 (oriented downslope, location in Fig. 1) highlights the three subsurface seismic horizons (named H1 to H3) from which surface maps were derived (Fig. 4) and shows upslope migrating sediment waves and cyclic steps, up to the seabed (SB). The unit above

H1 is named Upper Bedform Unit (UBU), the unit below H1 is named Lower Channelized System Unit (LCSU). Close-up in (c) shows details of SW; blue dashed arrows indicate the up-slope direction of migration.

Figure 3. (a) Arbitrary seismic profile L3 (oriented downslope, location in Fig. 4d) showing vertically stacked concave-up reflection packages that culminate in two topographic depressions at

the seabed. Arrows 4 to 8 point to high amplitude anomalies within the vertically stacked depressions; (b) detail of (a) showing trace representation of the main anomalies; (c) arbitrary seismic line L4 (oriented downslope, location in Fig. 4d) showing vertically stacked paleo-depressions and a series of sediment waves with an upslope direction of migration. Arrows 9 to 14 indicate positive and negative amplitude anomalies. The two insets on the right corner show the 3D architecture of anomalies marked by arrow 14. Colour scale indicates maximum brightness.

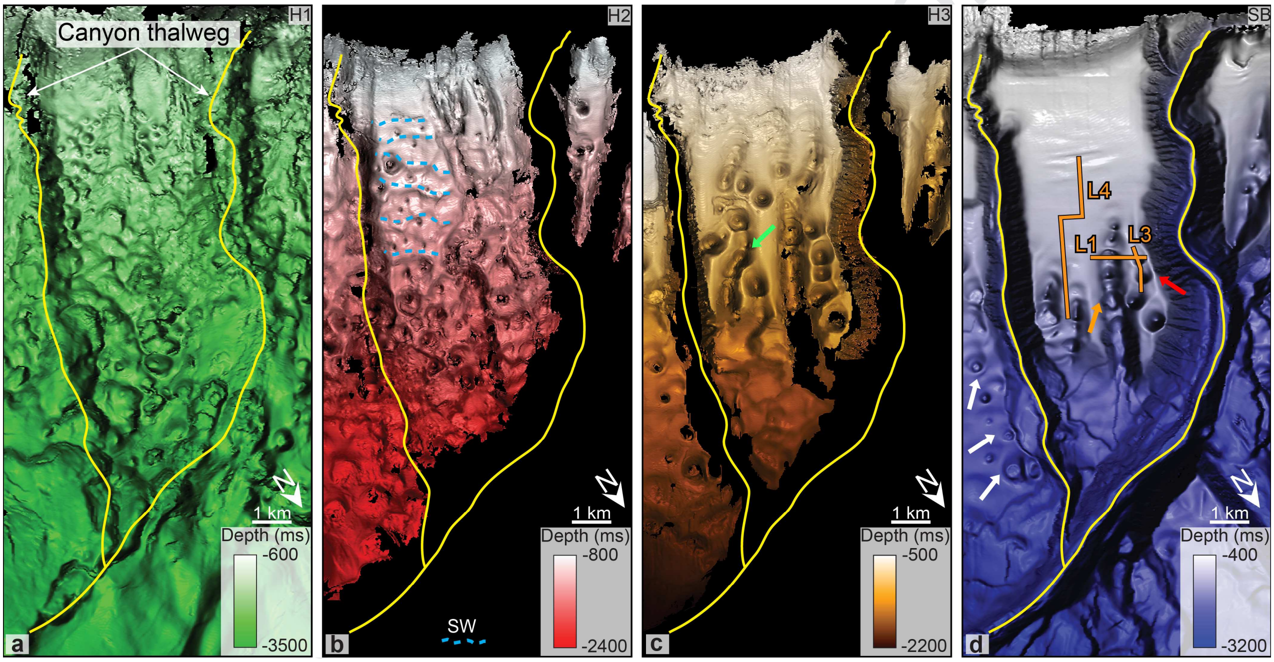

Figure 4. Time-structure maps of key horizons (location shown in Fig. 1): (a) H1, (b) H2, (c) H3, (d) seabed reflection (SB). Yellow lines indicate canyon thalwegs. Line L1 corresponds to the profile shown in Figure 2b, lines L3 and L4 to profiles shown in Figure 3. The green arrow in (c) indicates a trail of depressions, the white and red arrows in (d) indicate isolated circular depressions, and the orange arrow indicates a trail of elongated depressions.

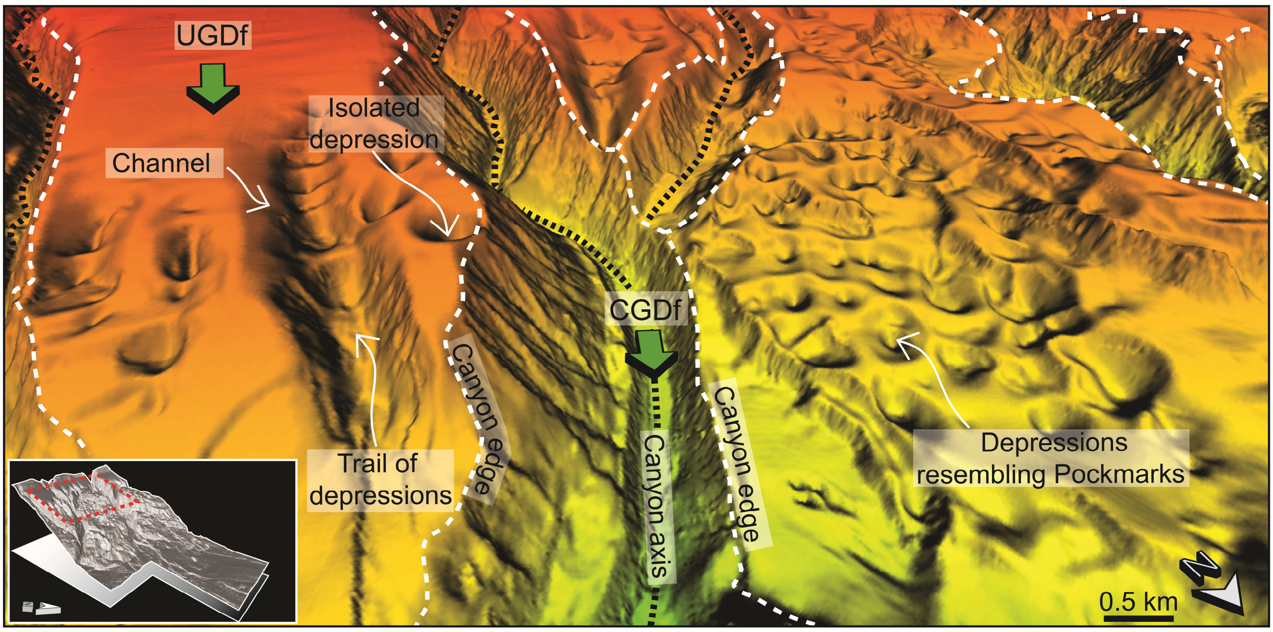

Figure 5. Perspective view of a portion of the time-structure map of the seabed (location in Fig. 1) illustrating the presence of large canyons, smaller channels, and widely distributed pockmark-shaped depressions, aligned in trails or standing as isolated features between the canyon edges. UGDf: Unconfined Gravity-Driven flows; CGDf: Confined Gravity-Driven flows.

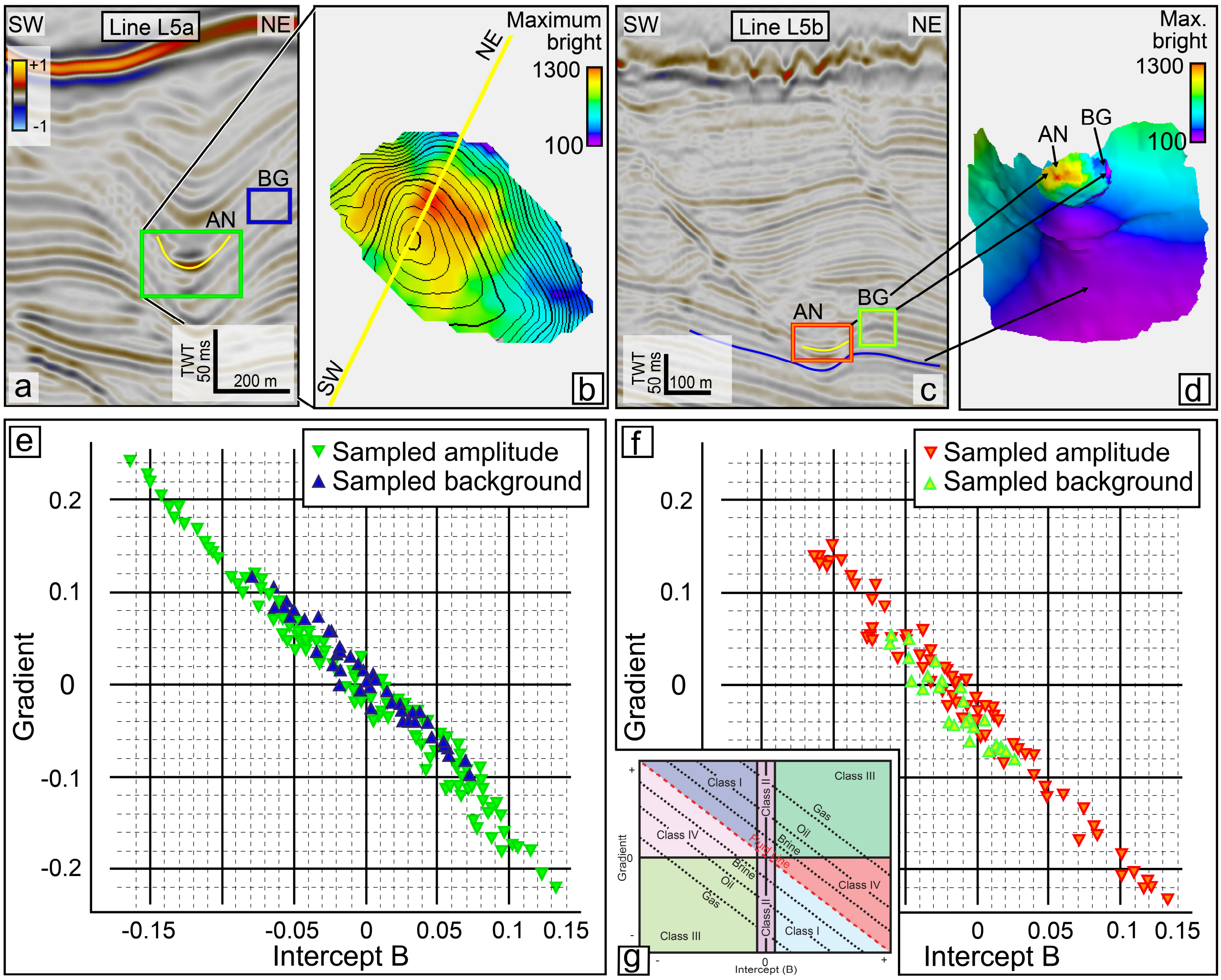

Figure 6: AVO analysis of selected amplitude anomalies using partial stack from lines L5a and L5b (Location in Fig. 1). (a) Seismic line L5a, the green rectangle indicates where an amplitude anomaly (AN) was sampled, the blue rectangle indicates where background (BG) amplitudes were sampled. (b) 3D mapping showing maximum bright values for amplitude anomaly shown in (a). (c) Seismic line L5b, red rectangle indicates the area where an amplitude anomaly (AN) was sampled, the green rectangle indicates where background (BG) amplitudes were sampled (d) 3D mapping showing maximum bright values for amplitude anomaly shown in (c). (e) Gradient versus intercept cross-plot of the amplitudes selected from (a). (f) Gradient versus intercept cross-plot of the amplitude selected from (c). (g) Schematic gradient versus intercept cross plot developed by Castagna and Swan, 1997; modified from Maestrelli et al., 2017.

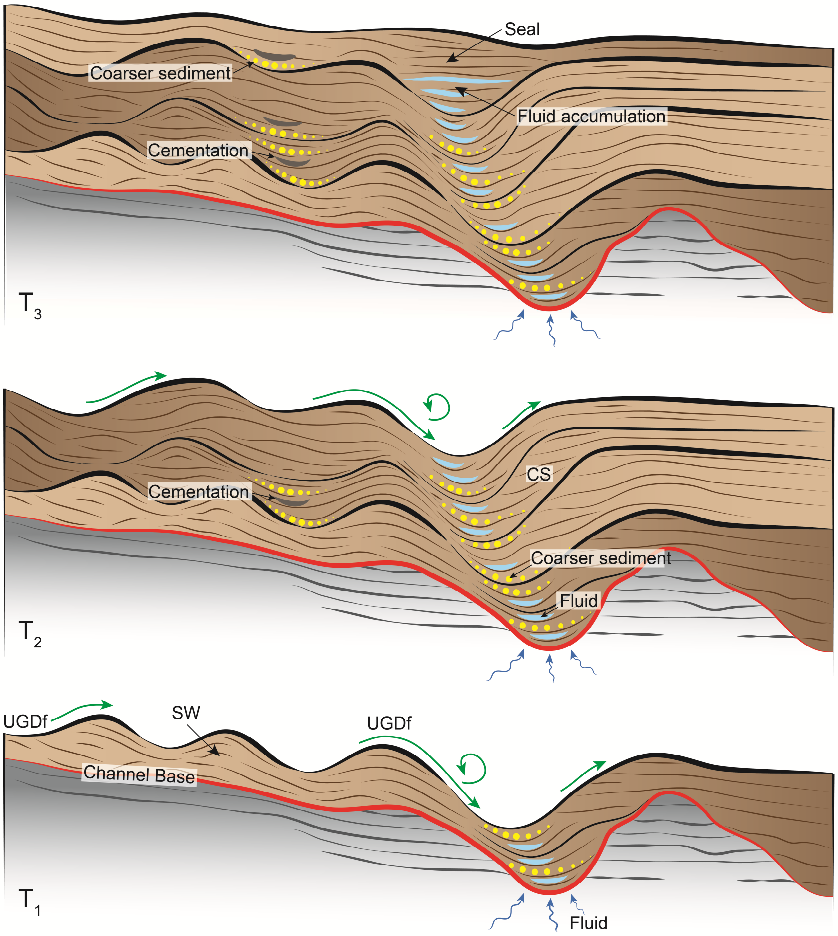

Figure 7. Schematic sketch (based on Fig. 3c) illustrating the proposed evolution of upslope-migrating sediment waves, the troughs of which stack over time so as to create a permeable pathway for fluid migration. In contrast to previous models for the migration of overpressured and hydrocarbon-rich fluids to form "advancing pockmarks", in our interpretation the passive migration of fluids takes places through natural fluid buoyancy. CS: Cyclic Steps; UGDf: unconfined Gravity-Driven flows; SW: Sediment Waves.

References

Aki, K. and Richards, P.G. (1980), Quantitative seismology: theory and methods. San Francisco. Freeman & Co.

Asmus, H.E., Porto R. (1972). Classification of Brazilian sedimentary basins according to plate tectonics. Congresso Brasileiro de Geologia 26, Belém (Ed.), Anais do XXVI Congresso Brasileiro de Geologia, 2, Sociedade Brasileira de Geologia, São Paulo (1972), pp. 67-90. (in Portuguese).

Avseth, P., Mukerji, T., and Mavko, G. (2010). Quantitative seismic interpretation: Applying rock physics tools to reduce interpretation risk. Cambridge university press.

Barrett et al, Near Surface Geophysics 2017, 15, 359-366

Bertoni, C., Gan, Y. P., Paganoni, M., Mayer, J., Cartwright, J., Martin, J., ... & Clare, A. (2019). Late Paleocene pipe swarm in the Great South–Canterbury Basin (New Zealand). Marine and Petroleum Geology.

Brown, A.R. (2004). Interpretation of three dimensional seismic data. 7th ed. AAPG Memoir, 42 American Association of Petroleum Geologists.

Cartigny, M.J.B., Postma, G., van den Berg, J.H., and Mastbergen, D.R. (2011). A comparative study of sediment waves and cyclic steps based on geometries, internal structure and numerical modelling. Marine Geology 280, 40-56. https://doi.org/10.1016/j.margeo.2010.11.006

Cartigny, M.J., Ventra, D., Postma, G., and van Den Berg, J.H. (2014). Morphodynamics and sedimentary structures of bedforms under supercritical-flow conditions: new insights from flume experiments. Sedimentology, 61(3), 712-748. https://doi.org/10.1111/sed.12076

Carvajal, C., Paull, C.K., Caress, D.W., Fildani, A., Lundsten, E., Anderson, K., ... and Herguera, J. C. (2017). Unraveling the Channel–Lobe Transition Zone With High-Resolution AUV Bathymetry: Navy Fan, Offshore Baja California, Mexico. Journal of Sedimentary Research, 87(10), 1049-1059. https://doi.org/10.2110/jsr.2017.58

Castagna, J.P. (1993). AVO analysis tutorial and review. In Offset dependent reflectivity –Theory and Practice of AVO analysis. Ed. J.P. Castagna and M.Bckus. Investigation in Geophysics N 8, Society of Exploration Geophysicists, pp 3-36.

Castagna, J.P., and Swan, H.W. (1997). Principles of AVO crossplotting. The leading edge, 16(4), 337-344. https://doi.org/10.1190/1.1437626

Condé, V.C., Lana, C.C., Pessoa Neto, O.C., Roesner, E.H., Morais Neto, J.M., and Dutra, D.C. (2007). Bacia do Ceará. Bol. Geoc. Petrobras 15, 347–355.

Covault, J.A., Kostic, S., Paull, C.K., Ryan, H.F., and Fildani, A. (2014). Submarine channel initiation, filling and maintenance from sea-floor geomorphology and morphodynamic modelling of cyclic steps. Sedimentology 61, 1031-1054. https://doi.org/10.1111/sed.12084

Davies, R.J. (2003). Kilometre-scale fluidization structures formed during early burial of a deep-water slope channel on the Niger Delta. Geology, 31-11, 949-952. https://doi.org/10.1130/G19835.1

Davison, I., Faull, T., Greenhalgh, J., Beirne, E., and Steel, I. (2016). Transpressional structures and hydrocarbon potential along fracture Zone: a review. Geological Society, London, Special Publications, 431(1): 235.

de Almeida, N.M. Vital, H., and Gomes, M.P. (2015). Morphology of submarine canyons along the continental margin of the Potuigar Basin, NE Brazil. Marine and Petroleum Geology 68, 307-324. https://doi.org/10.1016/j.marpetgeo.2015.08.035

Efthymiou, E., Morris, H., Wild. P., and Kemper. M. (2010). Seismic data conditioning of Partial Stacks. EAGE Extended abstract, earthdoc.eage.org.

Fildani, A., and Normark, W.R. (2004). Late Quaternary evolution of channel and lobe complexes of Monterey Fan. Marine Geology, 206(1-4), 199-223. https://doi.org/10.1016/j.margeo.2004.03.001

Fildani, A., Normark, W.R., Kostic, S., and Parker, G. (2006). Channel formation by flow stripping: Large-scale scour features along the Monterey East Channel and their relation to sediment waves. Sedimentology, 53(6), 1265-1287. https://doi.org/10.1111/j.1365-3091.2006.00812.x

Fildani, A., Hubbard, S.M., Covault, J. A., Maier, K.L., Romans, B. ., Traer, M., and Rowland, J.C. (2013). Erosion at inception of deep-sea channels. Marine and Petroleum Geology, 41, 48-61. https://doi.org/10.1016/j.marpetgeo.2012.03.006

Foster, D.J., Keys, R.G., Lane, D.F. (2010). Interpretation of AVO anomalies. Geophysics.75 (5): 75A3-75A13.

García, M., Hernández-Molina, F.J., Alonso, B., Vázquez, J.T., Ercilla, G., Llave, E., and Casas, D. (2016). Erosive sub-circular depressions on the Guadalquivir Bank (Gulf of Cadiz): Interaction between bottom current, mass-wasting and tectonic processes. Marine Geology, 378, 5-19. https://doi.org/10.1016/j.margeo.2015.10.004

Gay, A., Lopez, M., Berndt, C., and Seranne, M. (2007). Geological controls on focused fluid flow associated with seafloor seeps in the Lower Congo Basin. Marine Geology, 244(1-4), 68-92. https://doi.org/10.1016/j.margeo.2007.06.003

Hall, B., Meiburg, E. and Kneller, B. (2008). Channel formation by turbidity currents: Navier–Stokes-based linear stability analysis. Journal of Fluid Mechanics, 615, pp.185-210. https://doi.org/10.1017/S0022112008003467

Heggland, R. (1998). Gas seepage as an indicator of deeper prospective reservoirs. A study based on exploration 3D seismic data. Marine and Petroleum Geology, 15(1), 1-9. https://doi.org/10.1016/S0264-8172(97)00060-3

Heiniö, P., and Davies, R. J. (2009). Trails of depressions and sediment waves along submarine channels on the continental margin of Espirito Santo Basin, Brazil. Geological Society of America Bulletin 121, 698-711. https://doi.org/10.1130/B26190.1

Ho, S., Cartwright, J., & Imbert, P. (2012a). The formation of advancing pockmarks arrays: an interplay between hydrocarbon leakage and slope sedimentation. In Proceeding of American Association of Petroleum Geologists Annual Convention and Exhibition, Long Beach, USA (pp. 18-20).

Ho, S., Cartwright, J.A., and Imbert, P. (2012b). Vertical evolution of fluid venting structures in relation to gas flux, in the Neogene-Quaternary of the Lower Congo Basin, Offshore Angola. Marine Geology, 332, 40-55. http://dx.doi.org/10.1016/j.margeo.2012.08.011

Ho, S., Imbert, P., Hovland, M., Wetzel, A., Blouet, J.P., and Carruthers, D. (2018). Downslope-shifting pockmarks: interplay between hydrocarbon leakage, sedimentations, currents and slope's topography. International Journal of Earth Sciences, 107(8), 2907-2929. https://doi.org/10.1007/s00531-018-1635-5

Hovland, M. (2003). Geomorphological, geophysical, and geochemical evidence of fluid flow through the seabed. J. Geochem. Exploration, 78-79, 287-291. https://doi.org/10.1016/S0375-6742(03)00091-8

Hovland, M., Gardner, J.V., and Judd, A.G. (2002). The significance of pockmarks to understanding fluid flow processes and geohazards. Geofluids, 2(2), 127-136.

Hsu, S.K., Kuo, J., Chung-Liang, L., Ching-Hui, T., Doo, W.B., Ku, C.Y., and Sibuet, J. C. (2008). Turbidity currents, submarine landslides and the 2006 Pingtung earthquake off SW Taiwan. TAO: Terrestrial, Atmospheric and Oceanic Sciences, 19(6), 7.

Jobe, Z.R., Lowe, D.R., and Uchytil, S.J. (2011). Two fundamentally different types of submarine canyons along the continental margin of Equatorial Guinea. Marine and Petroleum Geology, 28(3), 843-860.

Jovane, L., Figueiredo, J.J., Alves, D.P., Iacopini, D., Giorgioni, M., Vannucchi, P., ... and Molina, E.C. (2016). Seismostratigraphy of the Ceará Plateau: Clues to Decipher the Cenozoic Evolution of Brazilian Equatorial Margin. Frontiers in Earth Science, 4, 90.

Judd, A., and Hovland, M., (2009). Seabed fluid flow: the impact on geology, biology and the marine environment. Cambridge University Press. New York, 492 pp

King, L.H., and MacLEAN, B.R.I.A.N. (1970). Pockmarks on the Scotian shelf. Geological Society of America Bulletin, 81(10), 3141-3148.

Krämer, K., Holler, P., Herbst, G., Bratek, A., Ahmerkamp, S., Neumann, A., ... & Winter, C. (2017). Abrupt emergence of a large pockmark field in the German Bight, southeastern North Sea. Scientific reports, 7(1), 5150.

Loncke, L., Mascle, J., and Parties, F.S. (2004). Mud volcanoes, gas chimneys, pockmarks and mounds in the Nile deep-sea fan (Eastern Mediterranean): geophysical evidences. Marine and Petroleum Geology, 21(6), 669-689.

Lonergan L., Jemin H. H., Jacson C. A., and Johnson, H.D. 2013. U-shaped slope gully systems and sediment waves on the passive margin of Gabon (West Africa). Marine Geology, 347, 80-97.

Løseth, H., Wensaas, L., Arntsen, B., Hanken, N. M., Basire, C., and Graue, K. (2011). 1000 m long gas blow-out pipes. Marine and Petroleum Geology, 28(5), 1047-1060.

Maestrelli, D., Iacopini, D., Jihad, A. A., Bond, C. E., and Bonini, M. (2017). Seismic and structural characterization of fluid escape pipes using 3D and partial stack seismic from the Loyal Field (Scotland, UK): a multiphase and repeated intrusive mechanism. Marine and Petroleum Geology, 88, 489-510. https://doi.org/10.1016/j.marpetgeo.2017.08.016

Matos, R.M.D., (2000). Tectonic evolution of the equatorial South Atlantic. W.U. Mohriak, M. Talwani (Eds.), Atlantic Rifts and Continental Margins, Geophysical Monograph, 115, American Geophysical Union. 331-354 https://doi.org/10.1029/GM115p0331

Mavko. G., Mukerji. T., and Dvorkin. J. (2012). The Rock Physics Handbook: Tools for Seismic Analysis of Porous Media. 4th Edition. Cambridge Press.

Meadows, D., and Davies, R.J. (2007). Morphological development of basin-scale silica diagenetic fronts revealed with two-dimensional seismic reflection data: Offshore Sakhalin, Russian Far East. Journal of the Geological Society, 164, 1193-1206.

Mohriak, W.U., M. Basseto, and I.S. Vieira, (2000). Tectonic Evolution of the Rifted Basins in the Northeastern Brazilian Region. In: W.Mohriak and M.Talwani, eds., Atlantic Rifts and Continental Margins: Geophysical Monograph 115, 293-315. https://doi.org/10.1029/GM115p0293

Mulder, T., and Syvitski, J. P. (1995). Turbidity currents generated at river mouths during exceptional discharges to the world oceans. The Journal of Geology, 103(3), 285-299.

Mulder, T., Weber, O., Anschutz, P., Jorissen, F., and Jouanneau, J.M., (2001). A few months-old storm-generated turbidite deposited in the Capbreton Canyon (Bay of Biscay, SW France). Geo-Marine Letters, 21(3), 149-156. Doi:10.1007/s003670100077

Normark, W.R., and Hess, G. R. (1980). Quaternary growth patterns of California submarine fans. In Field M.E. Bouma A.H. Colburn I.P. Douglas R.G. Ingle J.C., eds., Quaternary Depositional Environments of the Pacific Coast: Pacific Coast Paleogeography Symposium 4, Society of Economic Paleontologists and Mineralogists, Pacific Section , p. 201–21

Normark, W.R., Piper, D.J., Posamentier, H., Pirmez, C., and Migeon, S., (2002). Variability in form and growth of sediment waves on turbidite channel levees. Marine Geology 192, 23-58. https://doi.org/10.1016/S0025-3227(02)00548-0

Pilcher, R., and Argent, J., (2007). Mega-pockmarks and linear pockmark trains on the West African continental margin. Marine Geology 244, 15-32. https://doi.org/10.1016/j.margeo.2007.05.002

Plaza-Faverola, A., Bünz, S., & Mienert, J. (2011). Repeated fluid expulsion through sub-seabed chimneys offshore Norway in response to glacial cycles. Earth and Planetary Science Letters, 305(3-4), 297-308.

Puig, P., Ogston, A.S., Mullenbach, B.L., Nittrouer, C.A., Parsons, J.D., and Sternberg, R.W., (2004). Storm-induced sediment gravity flows at the head of the Eel submarine canyon, northern California margin. Journal of Geophysical Research: Oceans, 109(C3). Doi:10.1029/2003JC001918.

Ross, C.P., and Beale P.L., (1994). Seismic offset balancing. Geophysics, 59, 93-101. https://doi.org/10.1190/1.1443538

Symons, W.O., Sumner, E.J., Talling, P.J., Cartigny, M.J.B., and Clare, M.A., (2016). Large-scale sediment waves and scours on the modern seafloor and their implications for the prevalence of supercritical flows. Marine Geology, 371, 130-148. https://doi.org/10.1016/j.margeo.2015.11.009

Talling, P.J., Masson, D.G., Sumner, E.J. and Malgesini, G., (2012). Subaqueous sediment density flows: Depositional processes and deposit types. Sedimentology, 59, 1937-2003. https://doi.org/10.1111/j.1365-3091.2012.01353.x

Taner, M.T., Schuelke, J.S., O'Doherty, R., and Baysal, E. (1994). Seismic attributes revisited. In SEG Technical Program Expanded Abstracts 1994 (pp. 1104-1106). Society of Exploration Geophysicists. https://doi.org/10.1190/1.1822709

Taviani, M., Angeletti, L., Ceregato, A., Foglini, F., Froglia, C., and Trincardi, F. (2013). The Gela Basin pockmark field in the strait of Sicily (Mediterranean Sea): chemosymbiotic faunal and carbonate signatures of postglacial to modern cold seepage. Biogeosciences, 10, 4653-4671. https://doi.org/10.5194/bg-10-4653-2013

Veeken P.C.H. and van Moerkerken B (2013). Seismic Stratigraphy and Depositional Facies Models. EAGE publication, Houten, The nederlands, 493 pp. https://doi.org/10.1016/C2013-0-12810-3

Vital, H. Gomes, M.P., Tabosa, W.F., Frazao, E.P, Santos, C.L.A., and Placido Junior. J. S. (2010). Characterization of the Brazilian Continental shelf adjacent to Rio Grande do Norte State, NE Brazil. Braz. J. Oceanogr., 58, 43-54. http://dx.doi.org/10.1590/S1679-87592010000500005

Highlights

- 3D seismic data are used to examine near-seafloor features offshore Ceará, NE Brazil
- Depressions isolated or organised in trails are seen at and near seabed within a sediment succession recording downslope activity via canyons and channels
- AVO analysis exclude that the depressions were created by hydrocarbon seepage
- Depressions are interpreted as cyclic steps generated by gravity-driven flows,
- Cyclic steps formation provides pathways for passive fluid migration